Orbital hybridization in RVO_3 perovskites: A high-pressure study

J.-S. Zhou,[1,*] J. B. Goodenough,[1] J.-Q. Yan,[2] J.-G. Cheng,[1] K. Matsubayashi,[3] Y. Uwatoko,[3] and Y. Ren[4]
[1]*Texas Materials Institute, University of Texas at Austin, Austin, Texas 78712, USA*
[2]*Ames Laboratory, Ames, Iowa 50011, USA*
[3]*Institute for Solid State Physics, University of Tokyo, Kashiwa, Japan*
[4]*Advanced Photon Source, Argonne National Laboratory, Argonne, Illinois 60439, USA*
(Received 11 September 2009; revised manuscript received 17 November 2009; published 22 December 2009)

The RVO_3 perovskites undergo orbital ordering and orbital-flipping transitions as well as a spin ordering transition. However, the existing model of orbital ordering fails to explain the thermal conductivity, which remains poor and glassy in the orbitally ordered phase. The phonon thermal conductivity is restored only below a first-order orbital-flipping transition. Orbital ordering induces a specific lattice distortion, which makes uniaxial pressure suitable to distinguish and verify all possible orbital and spin orderings in orthorhombic RVO_3. We have made a systematic study of orbital/spin transitions in single-crystal samples of RVO_3 (R=Dy, $Y_{1-x}La_x$) under uniaxial and hydrostatic pressure. Comparison of the uniaxial and hydrostatic pressure effects on the spin/orbital-flipping transition permits us to identify orbital fluctuations due to the hybridization of t_2 and et orbitals in the type-G orbitally ordered phase.

DOI: 10.1103/PhysRevB.80.224422 PACS number(s): 75.30.Et, 75.40.Cx, 75.50.Ee, 75.30.Cr

I. INTRODUCTION

The interplay between spin, orbital and the structural-bias effect in 3d perovskite oxides has been actively discussed in recent years as it is an important element in the theory of superexchange interactions.[1–4] However, hard evidence leading to the precise microscopic picture is rare. Unlike the octahedral-site e-orbital Jahn-Teller (JT) systems where a cooperative lattice distortion lifts the orbital degeneracy at a significantly higher temperature than that for spin ordering, the orbital degree of freedom (ODF) in the t-orbital JT systems survives to low temperatures, which leads to interesting orbital dynamics caused by a competition between the orbital-orbital interaction, the spin-spin interactions, and the structural-bias effect. This competition brings about not only an orbital order-disorder transition, but also subsequent orbital-flipping transitions in RVO_3 perovskites. The state-of-the-art neutron-diffraction technique is unable to provide clear-cut evidence how the orbitals are ordered in this t-orbital system,[5–7] which forces us to find alternative probes to monitor changes of the ODF. We have demonstrated[8] with typical members of the RVO_3 perovskites that the thermal conductivity κ can be used to probe the entire evolution of orbital dynamics from a glassy phase to the phase in which the phonon structure is perfectly restored. In sharp contrast to the non-JT perovskites such as $RCrO_3$, κ in the t^1 $RTiO_3$ and t^2 RVO_3 systems is suppressed to the level of a glass in the paramagnetic phase below room temperature.[9] The phonon κ is restored below the Néel temperature T_N in $RTiO_3$ and $LaVO_3$,[10] which indicates that the ODF starts to be removed once spins are ordered. In the phase diagram of RVO_3 shown in Fig. 1, however, orbitals become ordered at a T_{oo} in the paramagnetic phase of the RVO_3 perovskites (R=Pr, Nd, …Lu).[11] The profile T_{oo} versus the rare-earth ionic radius (IR) coincides with the evolution of the local $VO_{6/2}$ site distortion, which indicates that the structural-bias effect plays an important role to induce the orbital ordering at T_{oo} in this t-orbital JT system. Without any justification, it has been assumed[5] that the xy orbital in this t^2 system is occupied at a temperature somewhere between room temperature and the melting temperature. The transition at T_{oo} is assumed to order another t electron into an out-of-phase arrangement along the c axis, i.e., yz in layer 1 and zx in layer 2. This orbital disorder-order transition picture, however, fails to explain the observation that the glassy $\kappa(T)$ just shows a very small slope change at T_{oo}.[8] The ODF appears to be reduced somewhat, but not to be quenched completely at T_{oo}. It is only at $T_{CG}<T_N$ where a transition from an out-phase arrangement (type-G orbital ordering) to an in-phase arrangement (type-C orbital ordering) along the c axis takes place, that the phonon κ is restored abruptly through a first-order transition in the RVO_3 perovskites (R=Dy, Y, Ho, …Lu). $DyVO_3$ is located at the boundary from the phase showing the transition at T_{CG} to the phase without T_{CG}. It has been shown that a reentrance transition to

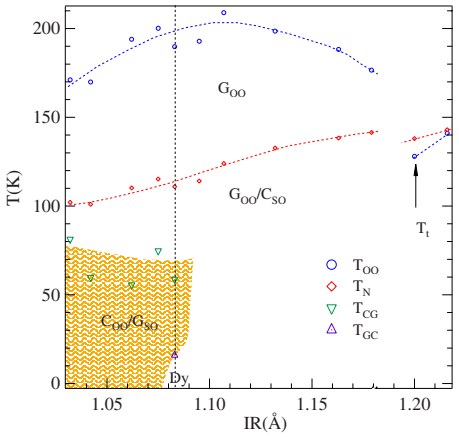

FIG. 1. (Color online) The phase diagram of RVO_3 perovskites, which illustrates the orbital order-disorder transition temperature T_{OO}, spin ordering temperature T_N, orbital-flipping transition T_{CG}, and the reentrance transition to type-G orbital ordering at T_{GC} as a function of the ionic radius of rare earths. Some data used in the diagram are from Ref. 7.

the out-of-phase (type-G) orbital ordering occurs at T_{GC} in $DyVO_3$.[12,13] Serial phase transitions from orbital disorder, to out-of-phase OO to in-phase OO and back to out-of-phase OO as temperature lowers indicates clearly that two driving forces compete to order the orbitals. The essential problem to be resolved in this study is why the thermal conductivity remains poor and glassy below the orbital ordering temperature, but is fully restored as in a regular crystal below a first-order orbital-flipping transition. We approach this problem by a systemic study of these orbital ordering/flipping transitions in single-crystal samples of $DyVO_3$ and $Y_{1-x}La_xVO_3$ under pressure. High-pressure studies on the orbital ordering in RVO_3 perovskites have been reported in the literature.[13,14] What is new in this study is that the results reveal all the detailed features of spin and orbital transitions under hydrostatic, quasihydrostatic, and uniaxial pressures. Moreover, the reentrance transition at low temperature in $DyVO_3$ allows us to check whether the poor thermal conductivity is always associated with the phase with out-of-phase orbital ordering, i.e., the orbital type-G phase (G_{oo}). The observation that the orbital-flipping transition splits into two transitions under pressure is a key for us to demonstrate that hybridization with the e orbital component is responsible for the poor thermal conductivity in the G_{oo} phase. We also note that the spin ordering in the C_{oo} phase requires the existence of an orbital angular momentum associated with the c-axis V-O-V bond, which has an unusual asymmetric covalent component of the V-O bonding.

II. EXPERIMENTAL DETAILS

The RVO_3 crystals were grown with the floating-zone method in an image furnace.[8] These crystals were characterized by x-ray powder diffraction and thermoelectric-power measurements in order to make sure that they are single phase and oxygen stoichiometric. The crystal orientation to major crystallographic axes in the samples used in the measurements under uniaxial pressure is within 1°. All magnetization measurements under hydrostatic/uniaxial pressure were carried out with miniature Be-Cu devices fitting into a commercial superconducting quantum interference device (SQUID) magnetometer (Quantum Design). Details about the device for the measurement under uniaxial pressure will be published elsewhere.[15] Two kinds of fluids were used as the pressure medium in the magnetization under hydrostatic pressure, silicone oil, and a mixture of 3M Fluorinert FC77 +FC72 (FC). The pressure inside the chamber was monitored by measuring the superconducting transition T_c of a small piece of Pb. The steady-state method was used in the measurement of thermal conductivity.

III. RESULTS

The $\kappa(T)$ of $DyVO_3$ has not been reported before. In order to show the relationship between the magnetic transitions and the corresponding changes of thermal conductivity κ, we have plotted in Fig. 2 the $\kappa(T)$ together with the magnetization $M(T)$ as well as the schematic drawings of spin and orbital orderings corresponding to the different phases. The

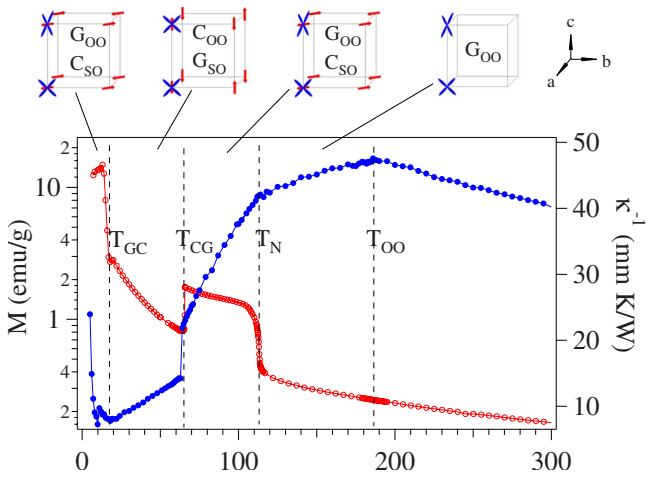

FIG. 2. (Color online) Temperature dependences of the magnetization M and the inverse thermal conductivity κ^{-1} of a $DyVO_3$ crystal. On top of the figure are schematic drawings of spin/orbital orderings corresponding to the different phases.

magnetization $M(T)$ shows dramatic changes at T_N, T_{CG}, and T_{GC}. No anomaly was found at the T_{oo} defined from a specific-heat measurement[11] since the $M(T)$ is dominated by the rare-earth moment in the paramagnetic phase of $DyVO_3$. In the RVO_3 perovskites with a nonmagnetic rare earth such as YVO_3 and $LuVO_3$, the orbital ordering at T_{oo} causes a slope change of $M(T)$.[16] Neutron powder diffraction has revealed unambiguously that the type-C spin ordering (C_{so}) occurs at T_N followed by a spin-flipping transition to the type-G AF ordering (G_{so}) at T_{CG} in YVO_3.[5–7] Based on the superexchange rules and the crystal symmetry, type-C orbital orderings $(C_{oo})/(G_{so})$ and the type-G orbital ordering $(G_{oo})/(C_{so})$ have been assumed in these spin-ordered phases. The G_{oo} phase is believed to be retained in the paramagnetic phase up to T_{oo}. The same spin/orbital transitions should also be applied to $DyVO_3$. Moreover, $DyVO_3$ shows an additional re-entrance transition to C_{so} at $T_{GC}<T_{CG}$. A collinear antiferromagnetic spin ordering of either type-C or type-G should not lead to a dramatic increase of $M(T)$. The abrupt changes of the $M(T)$ at T_N, T_{CG}, and T_{GC} found in $DyVO_3$ on top of a strong contribution from the magnetic moment at Dy^{3+} reflect a weak spin canting due to the Dzyaloshinsky-Moriya antisymmetric exchange interaction in the G_{oo}/C_{so} phase that is absent in the C_{oo}/G_{so} phase with spins parallel to the c axis.

A Curie-Weiss (CW) law fitting to the $M(T)$ of YVO_3 in the interval $T_N<T<T_{oo}$ gives a $\mu_{eff}=2.64\ \mu_B$ and a Weiss constant $\theta=-139$ K. These CW fitting parameters are reasonable for an $S=1$ antiferromagnet with $T_N\approx 120$ K. This result implies that the spin-spin interaction can be rationalized by the superexchange interaction through a classic orbital ordering below T_{oo}. The orbital angular momentum is essentially quenched. Although the G_{oo} phase below T_{oo} cannot be confirmed conclusively by neutron diffraction,[5–7] the $M(T)$, specific heat $C_p(T)$ and neutron-diffraction data all confirm a second-order phase transition at T_{oo}. As seen in Fig. 2, however, the orbital ordering, which provides the spin-spin interaction, does not restore the phonon thermal conductivity from the glassy phase above T_{oo}. The lattice

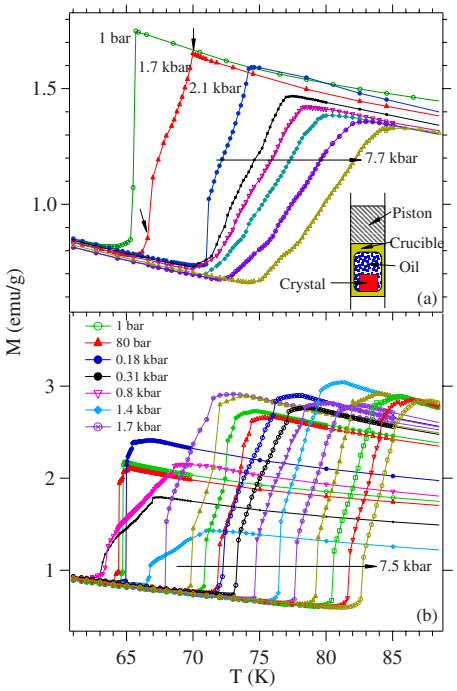

FIG. 3. (Color online) Temperature dependences of the magnetization of a $DyVO_3$ crystal under different pressures (a) with silicone oil as the pressure medium; (b) with FC as the pressure medium. Pressures corresponding to the curves at $P<2.1$ kbar are labeled inside plots. Pressures for the curves at $P>2.1$ kbar can be read from the temperature versus pressure in Fig. 4 The inset in (a) is a schematic drawing of the cell assembly.

randomness due to orbital fluctuations is further reduced at T_N before it is fully quenched at T_{CG}. The resolution of $\kappa(T)$ at low temperatures is high enough to reveal a change at $T_{GC}\approx 16$ K. Unfortunately, $\kappa(T)$ of a good-quality crystal normally peaks out near the same temperature. It is not sure whether the change of κ at T_{GC} is coincident or indicates a poor thermal conductivity in the G_{oo} phase below T_{GC}.

The pressure, especially uniaxial pressure, dependences can provide important information for understanding spin/orbital transitions in $DyVO_3$. In a previous publication,[13] we have reported the pressure dependence of T_N and T_{CG} for typical members in the whole RVO_3 family. In this paper, we focus on a comparison between the effects of hydrostatic pressure versus uniaxial pressure. Figure 3 shows the pressure effect on the first-order transition at T_{CG} with two different pressure media. Under ambient pressure, the transition is extremely sharp; it is finished within a $\Delta T\approx 0.1$ K. We start from the pressure effect with silicone oil as the pressure medium in Fig. 3(a). Upon applying pressure, the transition appears to split into two transitions, a higher $T_{CG}(U)$ and a lower $T_{CG}(L)$. It is also worth noting that the two transitions remain sharp until $P=2.2$ kbar. As pressure increases further, $T_{CG}(U)$ becomes more sensitive to pressure than $T_{CG}(L)$. One may wonder to what extent a nonhydrostatic component plays a role in broadening the transition at T_{CG}. In order to address this question, we have carried out the high-pressure experiment with the same setup on the same crystal; but the Teflon cell was filled with a mixture of 3M Fluorinert as the pressure medium, which provides hydrostatic pressure up to $P=9$ kbar. The first pressure point in the run with the silicone oil in Fig. 3(a) is at $P=1.7$ kbar; even with such a small pressure interval, we have still missed some very important information about the transition at T_{CG}. In the run with the Fluorinert, we initially increased the pressure with so small an interval that our pressure manometer could not distinguish between them. The pressures in this case were determined from the extension of a fitting curve of the pressure versus number of turns of the clamping screw in the pressure cell. The transition at T_{CG} actually includes a spin-flipping C_{so}/G_{so} transition that is accompanied by an orbital-flipping G_{oo}/C_{oo} transition and a first-order structural transition. These transitions may respond differently to high pressure. As shown in Fig. 3(b), the transition at T_{CG} remains sharp and shows a very small pressure dependence up to $P=0.2$ kbar. Remarkably, as pressure increases to 0.3–0.8 kbar, this transition spreads over a much broader temperature range. The initial run was terminated at $P=0.8$ kbar over concern that the crystal might be broken. The experiment was started over again after checking that the crystal was intact; the same broad transition under the same pressure range is repeatable. It is surprising that the transition, especially at $T_{CG}(L)$, becomes sharp again as seen in Fig. 3(a) for $P>1.4$ kbar. The transition under $P>1.4$ kbar resembles essentially the same features as those shown in Fig. 3(a). However, there are obvious differences caused by using different pressure media at higher pressures. This comparison makes clear that the transition at T_{CG} splits into two transitions and that this splitting has nothing to do with a broadening due to a nonhydrostatic pressure component. The pressure dependences of T_N and T_{CG} with different pressure media are summarized in Figs. 4(a) and 4(b). $T_{CG}(U)_$oil versus P obtained with the silicone oil is essentially identical to that of $T_{CG}(U)_$FC obtained with the Flurorinert. While $T_{CG}(L)_$FC is nearly parallel to $T_{CG}(U)_$FC as a function of pressure at high pressures, $T_{CG}(L)_$oil is much lower than $T_{CG}(U)_$FC at a given pressure. The information revealed by this experiment is critical for understanding the transition at T_{CG}. In our setup, an oriented crystal with the c axis parallel to the piston moving direction as shown in the inset of Fig. 3(a) was loaded in the pressure cell. Clustering of the oil under $P>2.2$ kbar may introduce a uniaxial pressure component along the c axis together with the hydrostatic pressure applied. A large difference between $T_{CG}(L)_$oil and $T_{CG}(L)_$FC reflects that $T_{CG}(L)$ is extremely sensitive to a uniaxial pressure along the c axis even if it is very small. Hydrostatic pressure increases $T_{CG}(L)$ as it does for $T_{CG}(U)$; but the uniaxial pressure along the c axis lowers $T_{CG}(L)$. These two effects on $T_{CG}(L)$ appear to cancel each other in the pressure range 2 kbar$<P<7$ kbar.

In order to confirm further the pressure effect on T_{CG}, we have measured the $M(T)$ near T_{CG} as the uniaxial pressure is applied along the c axis on the $DyVO_3$ crystal. As shown in a structural study,[17] the c axis shrinks a bit on heating through T_{CG} from the C_{OO} phase to the G_{OO} phase, which predicts a drop of the structural transition temperature if uniaxial pressure is applied along the c axis. Figure 5(d) shows results of $M(T)$ under uniaxial pressure along the c axis (it is also the direction of the applied magnetic field) of a $DyVO_3$ crystal. We have also plotted in Fig. 5(b) transi-

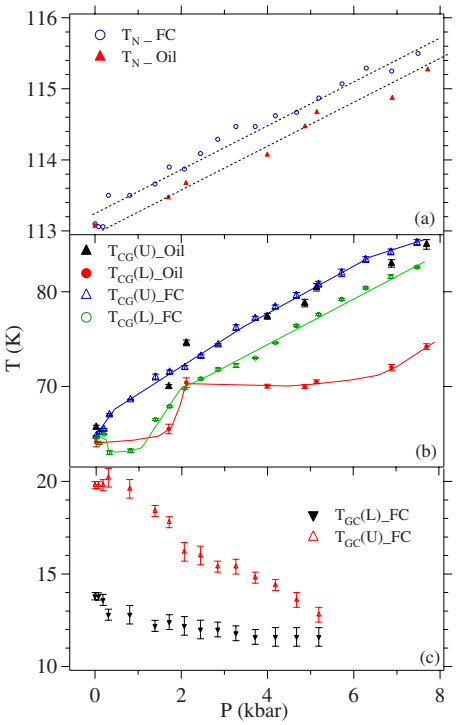

FIG. 4. (Color online) Pressure dependences of (a) Néel temperature T_N, (b) the orbital-flipping transition temperatures T_{CG} and (c) T_{GC} obtained by the high-pressure measurements on a $DyVO_3$ crystal with different pressure media, silicone oil (oil) and Fluorinert (FC).

tions at T_{CG}_FC under hydrostatic pressure for comparison. A small uniaxial pressure broadens dramatically the transition at T_{CG}; but it leaves $T_{CG}(U)$ more or less unchanged and shifts $T_{CG}(L)$ to low temperatures. Therefore, $T_{CG}(L)$ is strain sensitive. Both effects of hydrostatic and uniaxial pressures on the transition at T_{GC} in Figs. 5(a) and 5(c) are mirror symmetric to that at T_{CG}. Hydrostatic pressure suppresses the overall transition at T_{GC} and the transition vanishes finally under $P=7.5$ kbar. $T_{GC}(L)$ stays unchanged whereas $T_{GC}(U)$ moves to higher temperature under uniaxial pressure along the c axis.

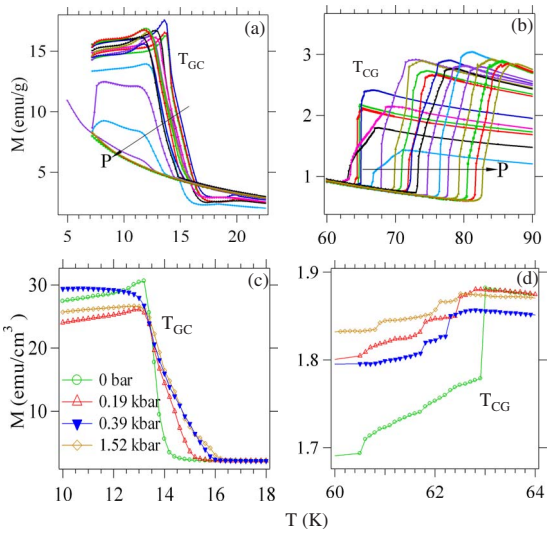

FIG. 5. (Color online) Temperature dependences of the magnetization of a $DyVO_3$ crystal. (a) In the vicinity of T_{GC} under hydrostatic pressure; (b) in the vicinity of T_{CG} under hydrostatic pressure; (c) in the vicinity of T_{GC} under c-axis uniaxial pressure; (d) in the vicinity of T_{CG} under c-axis uniaxial pressure.

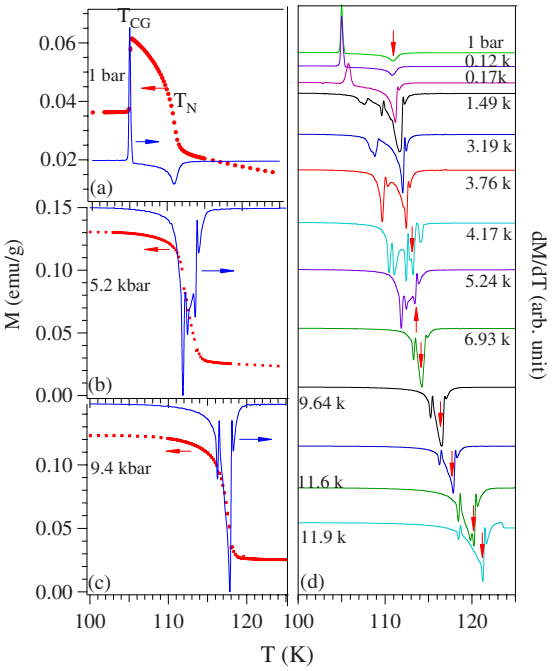

FIG. 6. (Color online) Temperature dependences of the magnetization M (a)–(c) and the dM/dT (d) of a $Y_{0.84}La_{0.16}VO_3$ crystal under different pressures. The label of the right axis in (a)–(c) is the same as in (d).

As seen from the phase diagram in Fig. 1, the orbital-flipping transition from G_{oo} to C_{oo} occurs below T_N, which means that the spin order could be a factor to alter the balance between different driving forces to order the orbitals. We also see from Fig. 4. that the magnitude of dT_{CG}/dP is much larger than that of dT_N/dP. Therefore, T_{CG} is expected to approach T_N under high pressure. The crossover of T_{CG} and T_N could induce spin-orbital interference. Unfortunately, the pressure capacity of the cell used is insufficient to fulfill this test on a $DyVO_3$ crystal. Like $DyVO_3$, YVO_3 exhibits all transitions except the reentrance transition at T_{GC}. Substituting La for Y increases T_{CG} and reduces T_N slightly.[18] Although a solid solution between YVO_3 and $LaVO_3$ can be obtained, the phase diagram does not answer unambiguously how T_{CG} approaches T_N. The problem remains open after a high-pressure structural study with synchrotron radiation on YVO_3 since T_N cannot be monitored by this method.[14] We have selected a composition $Y_{0.84}La_{0.16}VO_3$, which shows $T_N=111$ K and $T_{CG}=105$ K. This composition is ideal for us to fine tune these two transitions in a Be-Cu pressure cell that fits a commercial superconducting quantum interference device (SQUID) magnetometer.

Figure 6 shows three typical magnetization $M(T)$ and corresponding dM/dT curves of $Y_{0.84}La_{0.16}VO_3$ under different hydrostatic pressures. An abrupt increase of the magnetization below T_N indicates the type-C spin ordering with weak

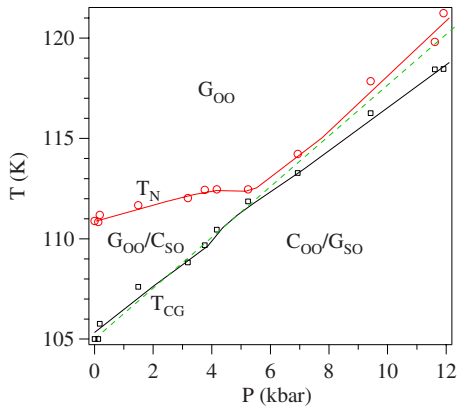

FIG. 7. (Color online) Pressure dependence of T_N and T_{CG} of a $Y_{0.84}La_{0.16}VO_3$ crystal.

spin canting. At ambient pressure, $M(T)$ behaves as a normal second-order transition at T_N and shows a first-order transition at T_{CG}. These two transitions combine under pressure. In order to track down in detail how the two transitions merge together, we have used anomalies in dM/dT versus T in Fig. 6(d) for different hydrostatic pressure P to define these transitions and show the evolutions of T_{CG} and T_N as a function of pressure. As in $DyVO_3$, the transition at T_{CG} broadens upon applying pressure. It should be noted that the behavior of $M(T)$ at T_{CG} changes from a drop to a jump on cooling as pressure increases further. At the same pressure, the transition at T_N becomes too sharp for a second-order transition. As T_{CG} approaches T_N, the whole transition of $M(T)$ becomes much broader and many anomalies in dM/dT versus T indicate multiple transitions take place. As pressure increases further, however, these anomalies combine into two minima again and both anomalies become much more pressure sensitive. A very weak anomaly of $dM(T)/dP$ at $T \geq T_N$ has been picked up in our measurement once pressure is applied. This anomaly stays for all pressures and appears to have no correlation with the changes of T_{CG} and T_N mentioned above.

There are three possibilities to interpret the relationship between T_{CG} and T_N under pressure: (1) T_{CG} simply crosses T_N; (2) T_{CG} and T_N are combined; (3) T_{CG} always stays below T_N to the highest pressure in this study. In the first case, the orbital-flipping transition at T_{CG} is no longer accompanied by spin ordering once T_{CG} is higher than T_N; the transition at T_{CG} would, therefore, produce a very small and broad change of $M(T)$ like that at T_{oo}. The observation of two clear anomalies of dM/dP to the highest pressure is against this solution. A single transition is expected in the second case, which is also not observed. Therefore, the third one is likely the solution and all pressure dependences in Fig. 7 have been labeled according to the last solution.

The volume change at T_{CG} is the main driving force for a large coefficient dT_{CG}/dP. T_N increases under pressure $P<5.5$ kbar with a slope $d \ln T_N/dP=3.3\times10^{-3}$/kbar, which is slightly larger than that found in RVO_3 (R=Dy, Y, and Lu).[13] However, the slope of T_N versus P increases abruptly to a giant $d \ln T_N/dP=1.1\times10^{-2}$/kbar at $P>5.5$ kbar where T_{CG} is close to T_N. The dashed line in Fig. 7 shows that the T_N versus P at $P>5.5$ kbar follows the extension to higher pressure of the first-order transition at T_{CG} versus P at $P<5.5$ kbar.

IV. DISCUSSION

Before making a detailed analysis of these pressure effects on T_{CG}, T_{GC}, and T_N, we interpret the phase diagram of Fig. 1 in the context of the competition between the structural-bias effect and the orbital-orbital interaction and highlight the possible origins of residual orbital fluctuations.

A. Structural-bias effect

The $GdFeO_3$-type distortion is commonly referred to as a prototype of the structural distortion in the orthorhombic perovskite with space group *Pbnm*. This structural distortion involves simply cooperative octahedral-site rotations that are proportional to the IR of rare-earth R^{3+} ion. We need to clarify how the structural distortions bias orbital ordering. Without considering the octahedral-site distortion, Mizokawa *et al.*[19] have shown that the C_{oo} phase is stabilized as the octahedral-site rotation increases. Our observation in Fig. 7 shows the opposite; high pressure favors the C_{oo} phase by reducing the site rotation. Moreover, the dome shaped Too versus IR in RVO_3 of Fig. 1 cannot be explained by the monotonic increase of the M-O-M bond angle from R=Lu to La. What we have to consider is the bias effect on orbital ordering by the local site distortions. The $MO_{6/2}$ site distortions associated with the octahedral-site rotations can be extracted from early-day single-crystal diffraction data and synchrotron and neutron-diffraction data for the $RFeO_3$ family.[20,21] These site distortions show three universal features in perovskites with orthorhombic *Pbnm* space group: (1) In the a-b plane, long and short O-M-O bonds alternate along the pseudocubic [100] and [010] axes; this site-distortion component is a maximum at an IR near that of Gd^{3+}. (2) With increasing IR from near the Gd^{3+} IR, the O_{21}-M-O_{22} bond angle α (see the definition in Fig. 8) that subtends the rotation axis b in the a-b plane decreases progressively from 90° as the first site-distortion component decreases so as to lower b relative a until they cross before the space-group symmetry changes from orthorhombic to tetragonal or rhombohedral. (3) As required by the *Pbnm* structural symmetry, the long and short O-M-O bonds in the a-b plane are in-phase on traversing the c axis. The in-phase bonding arrangement is more stable relative to the out of phase as the octahedral-site rotation increases, i.e., the IR decreases.

Let us check whether these intrinsic structural distortions bias the possible orbital orderings in this t^2 electron system. Ordering of two t electrons will create a long V-O bond inevitably. The example of Fig. 8(a) shows one electron ordered into the xy orbital and the other into the yz orbital; the long bond is along the y axis as indicated by double arrows. As shown in Fig. 8(b), the intrinsic site distortion derived from the structural data of the RVO_3 family at room temperature matches stunningly well the profile of T_{oo} versus IR, which clearly indicates the structural-bias effect on T_{oo}. However, the tendency to have the in-phase C_{oo} orbital order

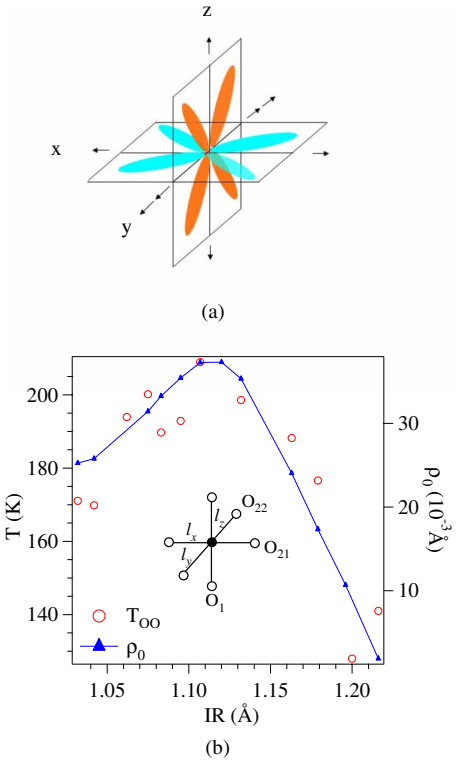

FIG. 8. (Color online) (a) A schematic drawing of the *xy* and *yz* orbital occupation at a V^{3+} site. (b) The IR dependence of the orbital ordering temperature T_{oo} and the site distortion ρ_0; where $\rho_0=(Q_2^2+Q_3^2)^{1/2}$; $Q_2=\ell_x-\ell_y$, $Q_3=(2\ell_z-\ell_x-\ell_y)/\sqrt{3}$.

along the *c* axis appears weaker below T_{oo} than the orbital-orbital interaction, which prefers the out-of-phase orbital ordering along the *c* axis. Stabilization of G_{oo} orbital order below T_{oo} demands a change of the space-group symmetry from *Pbnm*. Since the transition at T_{oo} is second-order, the G_{oo} space group must be a subgroup of *Pbnm*, such as $P2_1/a$ used in refining the neutron-diffraction data below T_{oo}.

B. Orbital-orbital interaction

The Heisenberg Hamiltonian describes the superexchange spin-spin interaction in a fixed orbital configuration. In dealing with the exchange interaction in a Mott insulator with orbital degeneracy, Kugel and Khomskii[22] (KK) have put forward a Hamiltonian that includes the intersite orbital-orbital interaction and the interference between the orbital and spin spaces as well as spin-spin interaction. As for the case of RVO_3, the out-of-phase orbital ordering along the *c* axis creates orbital overlaps between the empty and the occupied orbitals whereas the in-phase orbital ordering produces an uneven bonding of occupied to occupied and empty to empty. Coulombic repulsion is clearly against the in-phase orbital ordering, and this purely electronic consideration lifts the orbital degeneracy of in-phase versus out-of-phase orbital order.

Ordering the two t electrons, one into *xy* and the other into *yz* alternating with *zx* orbitals lowers the elastic energy in the 001 sheets; and the orbital-orbital interaction prefers the out-of-phase orbital ordering between the neighboring 001 layers below T_{oo}. As temperature lowers, however, the equilibrium *R*-O bond length decreases more than the equilibrium *M*-O bond length and an increased structural bias triggers the transition from the out-of-phase to the in-phase orbital ordering at T_{CG} at the expense of Coulombic energy. Spin ordering is another factor to shift the balance on the side of the structural-bias effect. The transition at T_{CG} is made possible only in the spin-ordered phase as shown in the phase diagram. A solid proof of this argument is from the experiment on the $La_{0.84}Y_{0.16}VO_3$ crystal where T_{CG} approaches T_N, but no crossover occurs under pressure. $DyVO_3$ is at the position where a fragile balance between competing effects is reached, which makes it possible for the orbital-orbital interaction to become dominant again at lowest temperatures, perhaps with help from ordering of the moment at Dy^{3+} at the reentrance transition back to the G_{oo} phase.[12]

Applying hydrostatic pressure and uniaxial pressure alters the balance in the competition so as to change the transition temperatures. At T_{CG} and T_{GC}, both spin and orbital flipping need not be first order. The only way to explain the volume change at the transition from the C_{OO} to the G_{OO} phase is that the site distortion in the G_{OO} phase has the $^3T_{1g}$ symmetry, which allows hybridization of t^2 and *et* configurations. Like the phase with a mixture of high-spin and low spin states in $RCoO_3$,[23] a lattice randomness due to the orbital hybridization contributes to the poor thermal conductivity in the G_{oo} phase below T_{oo}. The spin ordering at T_N optimizes the superexchange interaction through the *t*-O-*t* bonding and therefore reduces the hybridization. The first-order transition to remove the hybridization from the T_{CG} orbitals occurs at the orbital-flipping transition at T_{CG}. Pressure prefers the C_{oo} phase, which has a smaller cell volume, so it increases T_{CG} and suppresses T_{GC}. However, this does not explain why T_{CG} splits into two transitions under pressure. Hydrostatic pressure actually adds some frustrations to the competition between the structural bias at small R^{3+} IR and the orbital-orbital interaction. In light of the cell volume, hydrostatic pressure prefers the C_{OO} phase relative to the G_{OO} phase; therefore the pressure effect is on the same side as the structural bias. On the other hand, shrinking the unit cell in all directions, especially along the *c* axis, increases the coulomb energy in the C_{OO} phase relative to the G_{OO} phase. As a result, on cooling through T_{CG} the volume-sensitive transition, which eliminates the hybridization with the *e* orbital, occurs first at $T_{CG}(U)$. The transition from G_{OO} to C_{OO} follows the first-order elimination of the *e*-orbital hybridization at $T_{CG}(U)$ and is completed only at $T_{CG}(L)$. In other words, hydrostatic pressure splits the all-in-one transition at T_{CG} into the more volume-sensitive transition at $T_{CG}(U)$ and the *c*-axis strain sensitive transition at $T_{CG}(L)$. The results under *c*-axis uniaxial pressure in Fig. 5 provide a critical test for this argument. Since the hydrostatic and the uniaxial pressure effects on T_{GC} show a mirror symmetry to that of T_{CG}, all discussions about T_{CG} are applicable to T_{GC} as well.

In the experiments with silicone oil as the pressure medium, the pressure effect on T_{CG} appears to be due to a mixture of hydrostatic pressure and a *c*-axis uniaxial pressure. As pressure increases, the volume-sensitive transition at $T_{CG}(U)$ behaves exactly like that with the Fluorinert as the pressure medium. The nonhydrostatic component in silicone

oil emerges when the oil becomes clustered under a sufficiently high pressure. Since the c axis of the crystal is located parallel to the directional piston motion, the nonhydrostatic component in the pressure medium acts as a uniaxial pressure along the c axis. The hydrostatic pressure and the uniaxial pressure move $T_{CG}(L)$ in opposite directions, and these two effects appear to cancel each other at these pressures.

In the case of $Y_{0.84}La_{0.16}VO_3$, we can take advantage of a $dT_{CG}/dP > dT_N/dP$ to tune T_{CG} to where it approaches T_N continuously. In the circumstance of $T_{CG} \approx T_N$ under pressure, the possible interference between the orbital and spin spaces implied from the KK Hamiltonian finds a ground state to order both spins and orbitals like at T_N in $LaVO_3$ and $LaTiO_3$. In $Y_{0.84}La_{0.16}VO_3$, however, the much broader transition and multiple anomalies in Fig. 6 indicate that the interference does not result in a common ground state. We have concluded that hydrostatic pressure separates the volume-sensitive transition at $T_{CG}(U)$ from the c-axis strain sensitive transition at $T_{CG}(L)$. As these two transitions at $T_{CG}(U)$ and $T_{CG}(L)$ approach the magnetic transition under $P \approx 5$ kbar, the system becomes frustrated and multiple transitions are produced. At $P > 5.5$ kbar, the system appears to find a solution by combing the volume-sensitive transition with T_N and keeping the second-order orbital-flipping transition from G_{OO} to C_{OO} at a slightly lower temperature. Eliminating the e orbital component greatly enhances the spin-spin superexchange interaction through the t^2-O-t^2 bonding, which is an important driving force for a large dT_N/dP where the first-order transition combines with T_N. These arguments can be further supported by a numerical analysis. By simply increasing the orbital overlap integral under pressure, the Bloch's rule[24] can justify a $d \ln T_N/dP$ up to 1.6×10^{-3}/kbar based on the bulk modulus from a high-pressure structural study.[13] It is apparently not possible for the Bloch's rule to account for a large $d \ln T_N/dP = 3.3 \times 10^{-3}$/kbar at $P < 5.5$ kbar and a giant $d \ln T_N/dP = 1.1 \times 10^{-2}$/kbar at $P > 5.5$ kbar in Fig. 7.

The easy axis for spin ordering is the b axis in most perovskite magnets with the *Pbnm* space group. It is highly unusual to observe the G_{SO} with the easy axis along the c axis without any spin canting due to a site anisotropy in the C_{OO} phase below T_{CG}. One of the important factors contributing to this spin ordering is the uneven bonding formed in the in-phase orbital ordering where the π^* bond on oxygen is occupied in one direction and empty on turning 90°. This uneven bonding appears to be associated with a bond momentum that aligns spins on the V^{3+} ions along the bond axis even though a strong magnetostatic energy would order the spins in the a-b plane and the site rotations would favor a canting of the spins. Our results show that this unusual bonding state only occurs in the G_{so} phase. We call for attention from theorists to rationalize the relationship between the uneven bonding and evidence for an important bond orbital angular momentum.

V. CONCLUSIONS

$DyVO_3$ undergoes four transitions as it is cooled below room temperature. The orbital ordering transition at T_{oo} and orbital-flipping transitions at T_{CG} and T_{GC} are due to competition between the structural-bias effect and the orbital-orbital interaction. This scenario, however, does not explain why the orbital-flipping transition is first order. The high-pressure study in this report clarifies the situation as follows: (1) the behaviors of T_{CG} and T_{GC} under c-axis uniaxial pressure confirm the C_{oo} phase below T_{CG} and the G_{oo} phase below T_{GC}. (2) The first-order transition can be separated from the orbital-flipping transitions under hydrostatic pressure; the transition is likely associated with elimination of a hybridization of t^2 and et obitals in the G_{oo} phase. The orbital hybridization is responsible for the poor thermal conductivity in the orbitally ordered phase below T_{oo}. (3) In addition to the gain of the orbital overlap integral, high pressure reduces the e orbital component in the G_{oo} phase, which optimizes the superexchange interaction through the t-O-t bond so as to enhance greatly the coefficient $d \ln T_N/dP$ of the type-C spin ordering. (4) The interference between the orbital-flipping transition and spin ordering at T_N in $Y_{0.84}La_{0.16}VO_3$ does not result in a new ground state, but in multiple transitions where T_{CG} and T_N are merged together under pressure. (5) The C_{oo} phase has uneven c-axis bonding, i.e., empty to empty and occupied to occupied orbitals. At small R^{3+} IR, the structural-bias effect prefers the C_{oo} phase. We have shown that this peculiar bonding state can only be stabilized in the spin-ordered phase. This uneven electron bonding appears to play a role in forming an unusual easy c axis for spin ordering.

ACKNOWLEDGMENT

This work was supported by NSF (Grant No. DMR 0904282) and the Robert A Welch foundation (Grant No. F-1066) in USA and Grant-in-Aid for Scientific Research (Grant No. 21340092) from the Ministry of Education, Culture, Sports, Science and Technology in Japan.

*jszhou@mail.utexas.edu

[1] P. Horsch, A. M. Oles, L. F. Feiner, and G. Khaliullin, Phys. Rev. Lett. **100**, 167205 (2008).
[2] Y. Tokura, Phys. Today **56** (7), 50 (2003).
[3] G. Khaliullin, Prog. Theor. Phys. **160**, 155 (2005).
[4] D. I. Khomskii, J. Phys. A **36**, 9197 (2003).
[5] G. R. Blake, T. T. M. Palstra, Y. Ren, A. A. Nugroho, and A. A. Menovsky, Phys. Rev. Lett. **87**, 245501 (2001); Phys. Rev. B **65**, 174112 (2002).
[6] C. Ulrich, G. Khaliullin, J. Sirker, M. Reehuis, M. Ohl, S. Miyasaka, Y. Tokura, and B. Keimer, Phys. Rev. Lett. **91**, 257202 (2003).
[7] M. Reehuis, C. Ulrich, P. Pattison, B. Ouladdiaf, M. C. Rheinstadter, M. Ohl, L. P. Regnault, M. Miyasaka, Y. Tokura, and B.

Keimer, Phys. Rev. B **73**, 094440 (2006).
[8] J.-Q. Yan, J.-S. Zhou, and J. B. Goodenough, Phys. Rev. Lett. **93**, 235901 (2004).
[9] J.-G. Cheng, Y. Sui, J.-S. Zhou, J. B. Goodenough, and W. H. Su, Phys. Rev. Lett. **101**, 087205 (2008).
[10] J.-S. Zhou, Y. Ren, J.-Q. Yan, J. F. Mitchell, and J. B. Goodenough, Phys. Rev. Lett. **100**, 046401 (2008).
[11] S. Miyasaka, Y. Okimoto, M. Iwama, and Y. Tokura, Phys. Rev. B **68**, 100406(R) (2003).
[12] S. Miyasaka, T. Yasue, J. Fujioka, Y. Yamasaki, Y. Okimoto, R. Kumai, T. Arima, and Y. Tokura, Phys. Rev. Lett. **99**, 217201 (2007).
[13] J.-S. Zhou, J. B. Goodenough, J.-Q. Yan, and Y. Ren, Phys. Rev. Lett. **99**, 156401 (2007).
[14] D. Bizen, K. Nakatsuka, T. Murata, H. Nakao, Y. Murakami, S. Miyasaka, and Y. Tokura, Phys. Rev. B **78**, 224104 (2008).
[15] Y. Uwatoko (unpublished).
[16] Y. Ren, T. T. M. Palstra, D. I. Khomskii, A. A. Nugroho, A. A. Menovsky, and G. A. Sawatzky, Phys. Rev. B **62**, 6577 (2000).
[17] H. Kawano, H. Yoshizawa, and Y. Ueda, J. Phys. Soc. Jpn. **63**, 2857 (1994).
[18] J.-Q. Yan, J.-S. Zhou, J. B. Goodenough, Y. Ren, J.-G. Cheng, S. Chang, J. Zarestky, O. Garlea, A. Llobet, H. D. Zhou, Y. Sui, W. H. Su, and R. J. McQueeney, Phys. Rev. Lett. **99**, 197201 (2007).
[19] T. Mizokawa, D. I. Khomskii, and G. A. Sawatzky, Phys. Rev. B **60**, 7309 (1999).
[20] J.-S. Zhou and J. B. Goodenough, Phys. Rev. Lett. **94**, 065501 (2005).
[21] J.-S. Zhou and J. B. Goodenough, Phys. Rev. B **77**, 132104 (2008).
[22] K. I. Kugel and D. I. Khomskii, Sov. Phys. Usp. **25**, 231 (1982).
[23] J.-Q. Yan, J.-S. Zhou, and J. B. Goodenough, Phys. Rev. B **69**, 134409 (2004).
[24] D. Bloch, J. Phys. Chem. Solids **27**, 881 (1966).